Molecular Organization of the Tear Fluid Lipid Layer

Pipsa Kulovesi,[†△] Jelena Telenius,[¶△] Artturi Koivuniemi,[‖] Gerald Brezesinski,[**] Antti Rantamäki,[†] Tapani Viitala,[††] Esa Puukilainen,[‡] Mikko Ritala,[‡] Susanne K. Wiedmer,[§] Ilpo Vattulainen,[¶‖‡‡] and Juha M. Holopainen[†*]

[†]Helsinki Eye Lab, Department of Ophthalmology, [‡]Laboratory of Inorganic Chemistry, Department of Chemistry, and [§]Laboratory of Analytical Chemistry, Department of Chemistry, University of Helsinki, Helsinki, Finland; [¶]Department of Applied Physics, Aalto University, Aalto, Finland; [‖]Department of Physics, Tampere University of Technology, Tampere, Finland; [**]Max Planck Institute of Colloids and Interfaces, Potsdam, Germany; [††]KSV, Helsinki, Finland; and [‡‡]MEMPHYS-Centre for Biomembrane Physics, University of Southern Denmark, Odense, Denmark

ABSTRACT The tear fluid protects the corneal epithelium from drying out as well as from invasion by pathogens. It also provides cell nutrients. Similarly to lung surfactant, it is composed of an aqueous phase covered by a lipid layer. Here we describe the molecular organization of the anterior lipid layer of the tear film. Artificial tear fluid lipid layers (ATFLLs) composed of egg yolk phosphatidylcholine (60 mol %), free fatty acids (20 mol %), cholesteryl oleate (10 mol %), and triglycerides (10 mol %) were deposited on the air-water interface and their physico-chemical behavior was compared to egg-yolk phosphatidylcholine monolayers by using Langmuir-film balance techniques, x-ray diffraction, and imaging techniques as well as in silico molecular level simulations. At low surface pressures, ATFLLs were organized at the air-water interface as heterogeneous monomolecular films. Upon compression the ATFLLs collapsed toward the air phase and formed hemispherelike lipid aggregates. This transition was reversible upon relaxation. These results were confirmed by molecular-level simulations of ATFLL, which further provided molecular-scale insight into the molecular distributions inside and dynamics of the tear film. Similar type of behavior is observed in lung surfactant but the folding takes place toward the aqueous phase. The results provide novel information of the function of lipids in the tear fluid.

INTRODUCTION

Dry eye syndrome (DES) is the most common ocular disorder affecting ~10% of elderly individuals (1). Despite intensive research its pathophysiology has only very recently been somewhat revealed. DES is divided into aqueous deficient and evaporative forms of DES, of which the latter accounts for the majority of patients. DES is considered to arise from the interplay between an inadequate tear production, increased tear evaporation, and altered composition of the tear film. The underlying biochemical and physiological events in the development of DES remain only partly known. Yet it has become clear that the physical properties of the tear fluid and especially its lipid components are altered in DES. The composition of the human tear fluid is only partially known. Until now the model of the tear film has been a three-layered structure (2,3): The inner part is formed of a mucin-enriched layer adjacent to the epithelial cells, the middle aqueous layer is composed of soluble proteins and mucins forming a gel- and networklike structure, and the outermost layer consists of lipids (see Fig. S1 in the Supporting Material for a schematic representation of the anterior segment of the eye). It is believed that the lipids are secreted by the meibomian glands and are composed of both nonpolar and polar lipids (4,5). It has been suggested that, due to the hydrophobic effect, the polar phospholipids are disposed adjacent to the aqueous-mucin layer, whereas on top of this a layer composed of nonpolar lipids, such as cholesteryl esters (CEs) and triglycerides (TGs), faces externally the tear-air interface (6–8). This type of lipid organization is believed to strongly prevent evaporation. Nonetheless, this layerlike structure has not been proven experimentally.

Lipids can be either polar or nonpolar. Polar lipids are amphipathic, which means that they possess both hydrophilic and hydrophobic properties. This allows them to form bilayers, monolayers, vesicles, etc. in aqueous environment. Phospholipids, for example, have a hydrophilic headgroup and a hydrophobic fatty acid tail. Nonpolar lipids, such CEs and TGs, are hydrophobic. Due to their amphipathic nature, the phospholipids form a monomolecular layer on an air-water interface and reduce the surface tension. The properties of these monomolecular films depend strongly on, e.g., the chemical and molar composition, temperature, pH, ionic strength, and surface density (9). Nonpolar lipids are insoluble in polar solvents (such as water), but they readily dissolve in a nonpolar environment. If nonpolar lipids are deposited on an air-water interface, these molecules will not form a monomolecular film at the interface for energetic reasons, but instead will form three-dimensional aggregates. The surface behavior of mixtures of nonpolar and polar lipids is even more complex (10). As the composition and functional regulation of the tear fluid remain largely unknown, it is important to characterize the key factors of the homeostatic processes of the tear fluid, such as organization of lipids and viscoelasticity of the tear film.

Here we explore in detail the molecular level organization of an artificial tear fluid lipid layer (ATFLL) with an aim to

Submitted March 19, 2010, and accepted for publication June 28, 2010.

△Pipsa Kulovesi and Jelena Telenius contributed equally to this work.

*Correspondence: holopainen.juha@gmail.com

Editor: Douglas Nyle Robinson.

0006-3495/10/10/2559/9 $2.00

doi: 10.1016/j.bpj.2010.08.001

understand 1), how lipids of different polarity are deposited on the air-water interface; and 2), how the ATFLL accommodates and adapts the molecular organization of lipids during blinking.

MATERIALS AND METHODS

Materials

Egg phosphatidylcholine (eggPC) was obtained from Sigma (St. Louis, MO), and cholesteryl oleate (CO) and free fatty acids (FFA; 50% of stearic acid and 50% of palmitic acid) were from Fluka (Buchs, Switzerland). A mixture of TGs (including tricaprin, tricaprylin, trilaurin, tripalmitin, and trimyristin, 20% each) was bought from Supelco (Bellefonte, PA). Phosphate-buffered saline tablets were purchased from Medicago (Uppsala, Sweden). The purity of the lipids was verified by thin layer chromatography. Water was freshly deionized in a Milli RO/Milli-Q (Millipore, Bedford, MA) filtering system.

Samples

Samples (total molar concentration of 1 mM) consisted of either pure eggPC or a mixture of eggPC/FFA/CO/TG (60:20:10:10 mol %). The latter represented the ATFLL and is based on our unpublished lipidomic analysis of the tear fluid (J. M. Holopainen, A. Rantamäki, M. Jauhiainen, and M. Oresic, unpublished). Both samples were dissolved in chloroform.

Compression isotherms

Compression isotherms were measured using a Langmuir film balance (Minitrough; KSV, Helsinki, Finland) with a 20-mm paper probe. The solution of each lipid was spread in small aliquots onto a trough filled with 10 mM phosphate-buffered saline (0.140 M NaCl, 0.0027 M KCl, pH 7.4) at 21°C. The solvent was allowed to evaporate for 10 min. The monolayer films were compressed at a rate of 10 mm/min and compression was continued to a surface pressure of ~40 mN/m and then relaxed with the same rate. This compression-relaxation cycle was repeated twice for each monolayer.

Compressibilities of lipid monolayers

Phase transitions were determined using derivatives of surface pressure with respect to area (11). The values for monolayer isothermal compressibilities (C_S) for the indicated film compositions at the given surface pressures (π) were obtained from surface pressure-area (π-A) data by using Eq. 1,

$$C_s = \left(-\frac{1}{A_\pi}\right) * \left(\frac{dA}{d\pi}\right)_\pi, \quad (1)$$

where A_π is the area per chain at the indicated surface pressure. The data was further analyzed in terms of the reciprocal of isothermal compressibility (i.e., C_S^{-1}) (12). The higher the C_S^{-1} value, the lower the interfacial elasticity.

Oscillating barriers studies

A Langmuir film balance in the oscillating barrier mode was used for this study (KSV Minitrough). The oscillating barrier method allows a direct measurement of the amplitude of surface pressure oscillation due to infinitesimal changes in the monolayer area. With this method, the surface area covered by a monolayer is subjected to small periodic sinusoidal compressions by means of two oscillating barriers at a given frequency (ω) and amplitude ($\Delta A/A_\pi$), and the response of the surface pressure (π) was monitored.

The amplitude was maintained constant at 1%. The surface pressure was measured as above. The surface dilatational modulus is a complex quantity composed of a real and an imaginary part. It is derived from the change in surface pressure resulting from the small change in surface area and is described by

$$E = -(d\pi/d \ln A) = E_d + iE_v, \quad (2)$$

where the real part of the dilatational modulus (or the storage component) is the dilatational elasticity (E_d) and the imaginary part of the dilatational modulus is the surface dilatational viscosity (E_v). The tangent of the loss angle is given by

$$\tan \theta = E_v/E_d. \quad (3)$$

If the film is purely elastic, the loss angle tangent is zero.

Each sample was compressed to 30 mN/m and then relaxed back to 0 mN/m. This was repeated twice for all samples. After the last relaxation the film was compressed to 30 mN/m, and the monolayer was allowed to stabilize for 60 s before oscillation. Oscillation was first performed with a frequency of 200 mHz, followed by 100 mHz, 50, 25, 12.5, and 6.25 mHz. Eight oscillation cycles were made for each frequency. There was a waiting period of 60 s before each new oscillation. All measurements were performed in duplicates.

Grazing incidence x-ray diffraction

The lateral structures in condensed monolayers of pure eggPC or ATFLL mixture at the air/water interface were investigated using grazing incidence x-ray diffraction measurements (GIXD). The GIXD experiments were performed at the BW1 beamline, HASYLAB, DESY (Hamburg, Germany). The Langmuir film balance was thermostated (20°C) and placed into a hermetically closed container filled with helium. The Langmuir trough was equipped with a single movable barrier and a Wilhelmy plate for monitoring the lateral pressure. At BW1, a monochromatic x-ray beam ($\lambda = 1.304$ Å) strikes the water surface at a grazing incidence angle $\alpha_i = 0.85\alpha_c$ ($\alpha_c = 0.13°$) and illuminates roughly 2×50 mm^2 of the monolayer surface. During a diffraction experiment, the trough was laterally moved to avoid any sample damage by the strong x-ray beam. A linear position-sensitive detector (PSD, OEM-100-M; Braun, Garching, Germany) measured the diffracted signal and was rotated to scan the in-plane Q_{xy} component values of the scattering vector. The vertical channels of the PSD measured the out-of-plane Q_z component of the scattering vector between 0.0 and 0.9 Å^{-1}. The diffraction data consisted of Bragg peaks at diagnostic Q_{xy} values. The in-plane lattice repeat distances (d) of the ordered structures in the monolayer were calculated from the Bragg peak positions: $d = 2\pi/Q_{xy}$. To access the extent of the crystalline order in the monolayer, the in-plane coherence length (L_{xy}) was approximated from the full width at half-maximum (FWHM) of the Bragg peaks using $L_{xy} \sim 0.9(2\pi)/\mathrm{FWHM}(Q_{xy})$. The diffracted intensity normal to the interface was integrated over the Q_{xy} window of the diffraction peak to calculate the corresponding Bragg rod. The thickness of the monolayer was estimated from the FWHM of the Bragg rod using $0.9(2\pi)/\mathrm{FWHM}(Q_z)$. Experimental details are given in the literature (9,13–17).

Brewster angle microscopy

The morphology of the monolayer was visualized with a Brewster angle microscope (BAM1, Nanofilm Technology, Göttingen, Germany) mounted on a Langmuir film balance (R&K, Potsdam, Germany). The light source was a helium-neon laser (10 mW) at a wavelength of 632.8 nm. The diameter of the beam was 0.68 mm. After passing a polarizer, the p-polarized light was directed to the water surface under the Brewster angle (18–20).

The trough was placed on an antivibrational table (JAS, Affoltern, Switzerland). Image processing software was used to correct the BAM images for the distortion. The resolution of the BAM1 is ~4 μm.

Atomic force microscopy studies

For atomic force microscopy (AFM) studies a Multimode V with Nanoscope V controller (Veeco Instruments, Santa Barbara, CA) was used. Samples were measured in tapping mode in air using a phosphorus-doped silicon probe (RTESP; Veeco Instruments). Lipid films at the air-water interface were transferred to the surface of freshly cleaved mica using the Langmuir-Blodgett technique. The mica substrate was submerged through the air-water interface and the lipids were spread to the interface as described above. Before transfer, the lipid film was compressed and relaxed twice to the transfer surface pressure. The transfer was done at a controlled constant surface pressure by elevating the mica substrate through the air-water interface at a rate of 2 mm/min. Films were scanned by AFM within 24 h of transfer. Several scans were performed from different parts of the samples to check the uniformity of the surface. Final images were measured from a scanning area of 2×2 μm^2 with a scanning frequency of 0.5 Hz and no image processing except flattening was made.

Simulations

A detailed description of the simulation models and analysis of the simulation data is given in the Supporting Material. In brief, multicomponent lipid systems comprised of POPC, CO, FFA, trioleate (TRIOL), and water were modeled. For FFAs, two slightly different compounds, the saturated palmitic carboxylic acid and the monounsaturated oleate carboxylic acid were selected. All systems were described using the coarse-grained representation in terms of the Martini model (21,22). The initial structure of the model was based on a POPC-CO-POPC trilayer surrounded by water, where COs were embedded between the two POPC monolayers and the whole trilayer structure was solvated by a water phase (23). The system was copied twice to a simulation box, and some COs were removed from the middle of the two POPC monolayers to produce a vacuum region between the POPC layers. The layers were further pulled apart to increase the thickness of the vacuum region. Further, some COs were replaced by FFA molecules, and some of the POPC molecules were replaced by TRIOLs (24). The final lipid composition corresponded to a system of POPC/FFA/TRIOL/CO = 55:16:9:8 (in terms of the number of lipids in the model system). The force field for all the systems was based on the Martini model (Ver. 2.0) (21,22). In the oleate chains, the description was identical to the palmitoyl chain except for the third particle, which was assigned to the bead type C3 to describe the double bond. The simulations were carried out by using the GROMACS software package (Ver. 4.0.2) (25–27). The simulation temperature was maintained at 305 K with the Berendsen temperature coupling (28) using the time constant of 0.3 ps.

Radial distribution functions, mass densities, and order parameters as well as other physical observables were calculated from the simulation data with the GROMACS analysis tools, Ver. 4.0.4. The simulation results were visualized with VMD software. The pressure-area data for the equilibrium runs was fitted to experimental data presented in this article using the approach described by Baoukina et al. (29).

RESULTS

Compression isotherms and compressibilities of lipid monolayers

To begin, we compared the compression isotherm behavior of the ATFLL monolayers with purified eggPC monolayers. Pure eggPC monolayers were first spread on the air-water interface. Compression isotherms of eggPC monolayers did not show any discernible phase transition, and only a monotonous increase in the surface pressure-area (π-A) curve was seen (Fig. 1 *A*). The measured π-A isotherms closely resemble those of fluid PC monolayers (30). The monolayers were compressed to >40 mN/m with no evidence of film collapse. On relaxation, no hysteresis was observed (Fig. 1 *A*). In contrast, the compression isotherm for ATFLL monolayers showed a clear phase transition at ~18 mN/m and a small hysteresis behavior during the relaxation. The area/molecule at higher π-values (>10 mN/m) was considerably smaller for the ATFLL monolayers compared to the eggPC monolayers.

Pure eggPC monolayers showed liquid-expanded to liquid-condensed-like behavior during compression up to 40 mN/m, as evidenced by two distinctive slopes in the C_S^{-1}-A curve, as well as the absolute values of C_S^{-1} (Fig. 1 *B*). The C_S^{-1} value for the liquid-expanded phase is typically between 10 and 50 mN/m, whereas liquid-condensed phases have values >100 mN/m (31). The C_S^{-1} values were much lower for the ATFLL monolayers compared to the eggPC monolayers (Fig. 1 *B*). The C_S^{-1} values for the ATFLL monolayers suggest that the monolayers show liquid-expanded-like behavior during compression up to 40 mN/m. The local maximum and the sudden drop in the C_S^{-1}-A curve for the ATFLL monolayers can be attributed to the completion of the phase transition that was also seen in the compression isotherms. No hysteresis effect in the C_S^{-1}-A curves was found for either of the monolayers.

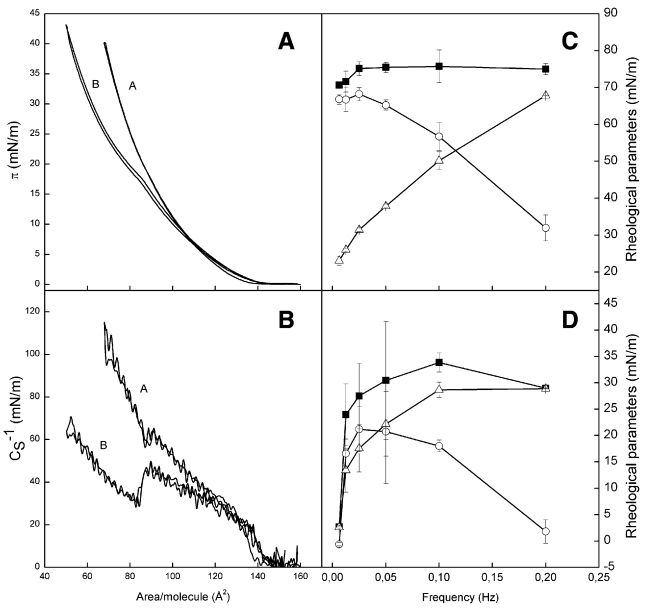

FIGURE 1 (*A*) Representative compression and relaxation isotherms for eggPC (trace *A*) and ATFLL (trace *B*). (*B*) The C_S^{-1} versus mean molecular area for eggPC (trace *A*) and ATFLL (trace *B*). Effect of frequency on rheological parameters (■, E; ○, E_d; Δ, E_v) for eggPC (*C*) and for ATFLL (*D*). All experiments were done in duplicates. The experimental details are given in the text.

Surface dilatational rheology of lipid monolayers

Trough methods are preferable methods for measuring surface dilatational rheological parameters (e.g., surface dilatational moduli (E), its elastic (E_d) and viscous (E_v) components, and loss angle tangents) for insoluble films at the air-water interface. The mechanically generated oscillating sinusoidal compressions and expansions of the barriers at a given frequency in a Langmuir film balance produce a longitudinal wave, and causes a response in the surface tension which is then monitored. The surface viscoelastic properties of eggPC monolayers spread on the air-water interface at $\pi = 30$ mN/m as a function of frequency (f) over a range of 6.25–200 mHz are shown in Fig. 1 *C*. A small increase in E was observed as f was increased from 6.25 mHz to 25 mHz. E and E_d were found to be essentially the same at $f \leq 25$ mHz. However, at $f > 25$ mHz, E_d decreases with concomitant increase in E_v, and the value of E_v increased with f and exceeded that of E_v at higher frequencies ($f > 100$ mHz). Accordingly, it can be concluded that eggPC monolayers present rheological behavior in dilatational conditions that are essentially elastic at low frequencies ($f < 25$ mHz) and viscoelastic at higher frequencies ($f > 25$ mHz). As a consequence of the viscoelastic behavior, the loss tangent angle (tan θ) increased with frequency (Fig. 2). The rheological behavior of ATFLL monolayers was more complex. E was found to be much lower than for eggPC monolayers and showed viscoelastic behavior over the whole frequency range of 6.25–200 mHz (Fig. 1 *D*). The values of E_d and E_v were essentially the same up to a frequency of 50 mHz, whereafter E_d exceeded that of E_v. Concomitantly, tan θ was always larger for the ATFLL monolayer compared to the eggPC monolayer (Fig. 2). The tan θ for the ATFLL monolayer showed a minimum at a frequency of 25 mHz, which did not appear for the pure eggPC monolayer. After the minimum, the tan θ increased with f with approximately the same slope as for the eggPC monolayer, but with an offset of 0.4 compared to the eggPC monolayer.

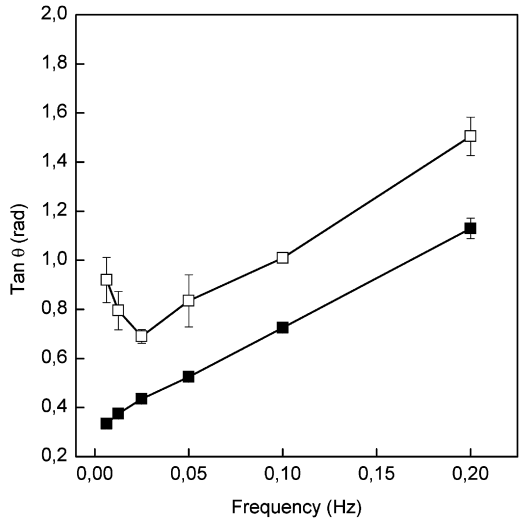

FIGURE 2 The loss of tangent θ as a function of frequency for eggPC (■) and ATFLL (□).

X-ray diffraction studies of lipid monolayers

Pure eggPC monolayers are in a fluidlike state and do not show long-range ordering. Therefore, no Bragg peaks were seen in the GIXD experiments. Meanwhile, the ATFLL mixture showed a clear Bragg peak at 1.507 Å^{-1} with FWHM of 0.013 Å^{-1} (Fig. 3). Additionally, there was a weak hint of a broad halo centered at ~1.3 Å^{-1} (Fig. 3, *inset*). This halo is more pronounced in other mixtures, which will be described elsewhere. Because the halo is only observed in the presence of CO, it is obvious that the CO has a condensing effect on the eggPC. This condensing effect could be described as the formation of liquid-ordered domains within the monolayer. If CO is not in the sample, the halo cannot be seen. In our case, the CO concentration is only 10 mol %, therefore the halo is very weak.

Taking into account that the instrumental resolution is 0.008 Å^{-1}, the FWHM of the Bragg peak leads to a correlation length of 565 Å. The Bragg peak should arise from FFA and/or TG. Because a single Bragg peak is observed, the condensed part of the monolayer exhibiting ordering should be a homogeneous mixture. In the nontilted and hexagonally packed LS phase, a pure stearic acid monolayer, which has a phase sequence L_2 – Ov – LS, exhibits a single Bragg peak at 1.518 Å^{-1}. The cross-sectional area of the hydrocarbon

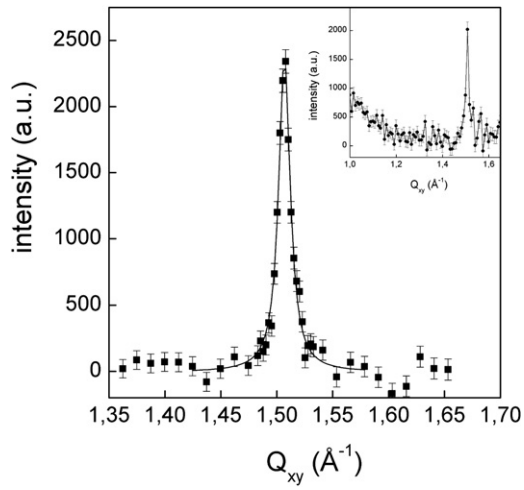

FIGURE 3 Diffracted intensity, corrected for polarization, effective area, and Lorentz factor, versus the in-plane component Q_{xy} of the scattering vector measured at 20 mN/m for the ATFLL mixture. The measured intensity is integrated over a Q_z range from 0 to 0.4 Å^{-1}. The horizontal resolution of 0.008 Å^{-1} was determined by a Soller collimator mounted in front of the PSD. A Lorentzian model peak was least-square-fitted to the measured intensities of the Bragg peak. (*Inset*) Broader Q_{xy} range to show the additional broad halo.

chains amounts to 19.8 Å^2. Palmitic acid has the same phase sequence with a slightly larger cross-sectional area. The transition into this nontilted state occurs at 24.2 mN/m for stearic acid and at 22.4 mN/m for palmitic acid. In our case, GIXD experiments were performed at 20 mN/m. The length of a hydrocarbon chain in all-*trans* conformation with n CH_2 groups can be calculated according to $l_{max} = (n \times 1.26 + 1.5)$ Å. The hydrocarbon chain of stearic acid has a length of 21.7 Å and that of palmitic acid of 19.1 Å. In the case of a pure stearic acid monolayer in the LS phase, the measured FWHM(Q_z) amounts to 0.26 Å^{-1} (the vertical instrumental resolution is negligible in this case), giving a thickness of 21.7 Å, which is in perfect agreement with the calculated value. In our case, the Bragg rod cannot be quantitatively analyzed because of the weak intensity, but we do not have any evidence for a tilted phase. This means that already at 20 mN/m the condensed phase observed is the LS-phase. This could be due to the mixing of FFA and TG.

Brewster angle microscopy lipid monolayers

The eggPC monolayer showed a typical fluidlike behavior with no visible pattern seen in the BAM images (not shown). The ATFLL monolayer was at all pressures inhomogeneous (not shown). Bright spots representing thicker areas were observed even at the lowest pressure. Compared with the GIXD results, these bright spots should therefore describe demixed condensed FFA/TG islands produced already during the spreading process.

Atomic force microscopy of lipid monolayers

AFM was used to complement the BAM results because it provides a convenient means to explore the three-dimensional organization of eggPC and ATFLL monolayers. BAM showed that the ATFLL monolayers were not homogenous in two dimensions, but it provided no evidence of whether the lipids were deposited on the air-water interface as a single monolayer. Accordingly, we chose to use AFM to explore this view. The lipids were deposited to the air-water interface and then transferred to mica substrates at surface pressures of 20 and 30 mN/m. At both surface pressures, eggPC films were rather homogenous, except for regions of membranes with small holes (not shown). Despite the holes, eggPC monolayers showed no evidence of multilayer formation. Similar holes could also be found in ATFLL films. Yet, ATFLL films showed clearly that the mixtures were nonhomogenous and that the lipid films formed protruding multilayered aggregates on the surface of the lipid membrane (Fig. 4).

Simulation results

The structure of a lipid layer changes as a function of lateral pressure. This effect was rationalized by simulating the lipid

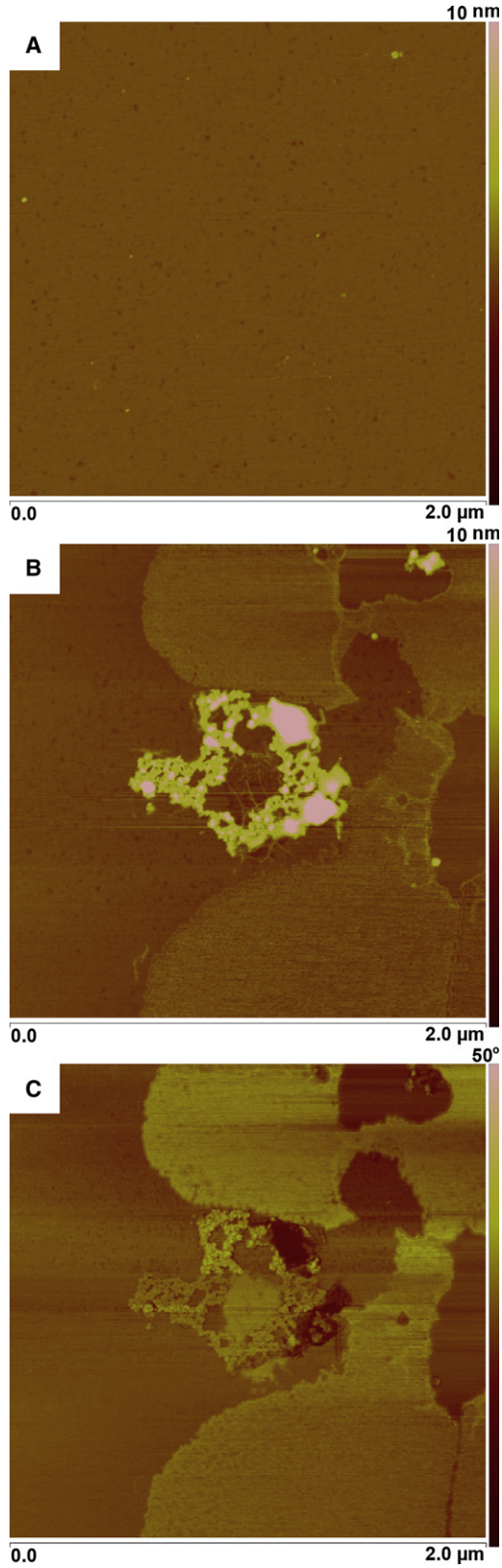

FIGURE 4 AFM topography images of eggPC (*A*), ATFLL (*B*), and phase image of ATFLL (*C*) attached to mica surface at 20 mN/m.

system with different molecular areas (in the *x-y* plane). Five systems with areas per lipid ranging from 42.1 to 64 Å^2/lipid were modeled. The corresponding surface pressures were calculated by scaling the data to match experimental results (29), and the surface pressures ranged from 15 mN/m to 50 mN/m.

The lipid layer structure changed substantially with an increase in pressure, as illustrated in Fig. 5, which shows snapshots of systems at various surface pressures. Below, we summarize our main findings using the data for density profiles along the membrane normal. Additional results for radial distribution functions and a number of other quantities are in line with these observations and will be discussed in detail elsewhere (J. Telenius, P. Kulovesi, A. Koivuniemi, G. Brezesinksi, J. M. Holopainen, and I. Vattulainen, unpublished).

The density profiles of POPC and FFA in the lipid layer showed no substantial dependence on surface pressure (Fig. 6). Nevertheless, the area/lipid POPC and FFA were located at the water-lipid interface with their hydrophobic chains pointing toward the air phase. The choline group of POPC was outermost and deeper in the water phase than the carboxyl group of FFA, which was located at the same level as the glycerol group of POPC. The picture given by POPC and FFA distribution at the surface layer is therefore consistent with typical findings for lipid monolayers at the air-water interface.

The distribution and orientation of CO and TRIOL showed a different behavior. For the largest area (64 Å^2/lipid), the CO and TRIOL molecules were located slightly farther away from the water phase than POPC and FFA, with the ester group of CO and the glycerol group of TRIOL just below the carboxyl group of FFA, pointing toward the air phase. For decreasing area, TRIOL molecules and some of the CO molecules were turned around to have their glycerol and ester groups in the air-lipid interface, and TRIOL chains clustered with CO molecules to phase-separate from the POPC-FFA layer at the water surface. Further, CO molecules in part circulated dynamically between the air-lipid and water-lipid interfaces. These trends initiated already at the area of 56.7 Å^2/lipid and were gradually promoted as the area per lipid decreased. The phase separation became essentially complete at the smallest area (42.1 Å^2/lipid), in which case CO and TRIOL formed a separate, hemispherelike structure over the POPC-FFA-layer. This finding is highlighted by the density profiles shown in Fig. 6.

The balloonlike cluster comprised of CO and TRIOL was separated from the water phase by a complete POPC-FFA layer. One small region of the surface, which also included a small part of the CO-TRIOL cluster, was located under the surface layer. Thus, as almost all CO and TRIOL molecules were displaced from the water-lipid surface, the surface area available for the hydrophilic headgroups of POPC and FFA was still large despite the small area per chain. The POPC-FFA layer on the top of the CO-TRIOL cluster had a bilayerlike structure. However, many FFA molecules in the POPC-FFA layer were turned upside down, i.e., the carboxyl groups were in contact with the ester groups of the CO molecules on the surface of the CO-TRIOL cluster, while hydrocarbon chains were in the POPC-FFA layer.

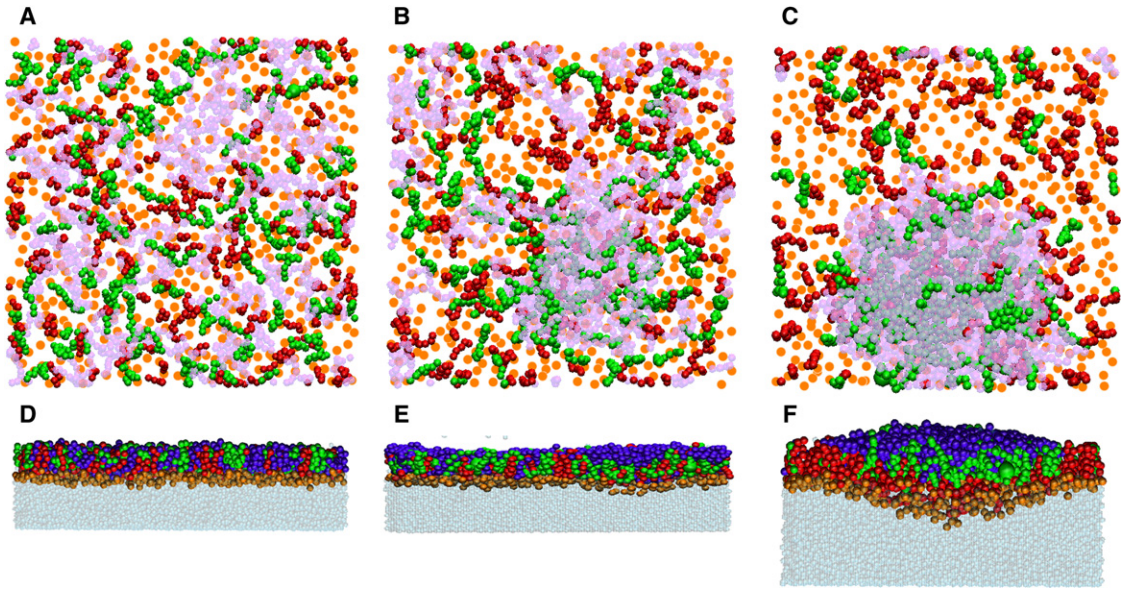

FIGURE 5 Snapshots from molecular simulations illustrating the formation of TG- and CE-rich clusters to the air side of the interface at high surface pressures (small areas per lipid). (*A–C*) Lipid layer illustrated from the air phase with an area per lipid of (*A*) 64 Å^2, (*B*) 53.1 Å^2, and (*C*) 42.1 Å^2. POPC headgroups are shown in orange, TG in pink mesh, CE in green, and FFA (palmitate) in red. (*D–F*) Lipid layer depicted from the side, the water phase being below the layer. The area per lipid is (*D*) 64 Å^2, (*E*) 53.1 Å^2, and (*F*) 42.1 Å^2. POPC headgroups are shown in orange, TG in blue, CE in green, FFA (palmitate) in red, and water in gray mesh. In all plots for POPC, only the headgroup choline is shown; for other molecules, the coloring is for the whole molecule.

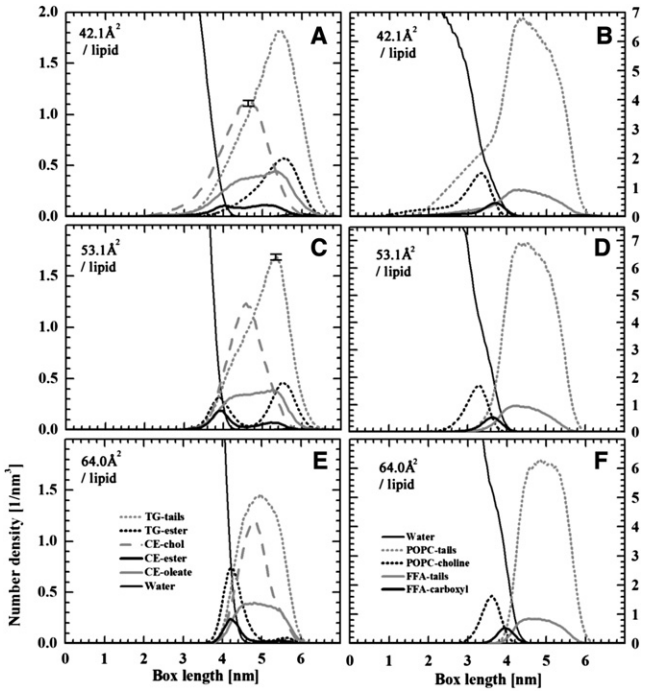

FIGURE 6 Distributions of number densities along the layer normal direction. The length scale on the *x* axis ranges from 0 to 7 nm such that the peak of POPC tails has a maximum at approximately the same position in all systems shown here. Water is on the left- and air on the right-hand side of the lipid layer. (*A*, *C*, and *E*) The distributions of POPC and FFA (palmitate), the curves representing the center of mass of the hydrocarbon chains as well as the headgroup carboxyl of FFA and the choline of POPC. (*B*, *D*, and *F*) The distributions of TG and CE, the curves here representing the center of mass of the hydrocarbon chains as well as the ester group of CE and the ester groups of TG. The distributions highlight the formation of hills on the water side of the layer for decreasing area per lipid.

In the balloonlike CO-TRIOL cluster, the glycerol groups of TRIOL were located in the plane of the layer, close to the air-lipid interface, and the CO molecules and the hydrophobic parts of TRIOL induced the ballooning effect to the side of the water-lipid interface. Some TRIOL acyl chains were also found at the air-lipid interface. Moreover, some FFAs were observed in the cluster region too—the carboxyl groups of these FFAs interact with the glycerol groups of trioleates.

DISCUSSION

Here we have analyzed in detail the molecular organization of a model of ATFLL and furthermore considered the physical changes in the ATFLL during compression and relaxation of the film, i.e., in similar condition as in blinking. Based on our previous findings (32) and our unpublished lipidomic profiling (J. M. Holopainen, A. Rantamäki, M. Jauhiainen, and M. Oresic, unpublished), the main component of the lipid film is amphipathic phospholipids, which lie adjacent to the tear-air interface. This layer acts as a surfactant to form a spreading interface between the aqueous phase and the hydrophobic layer. A layer of nonpolar lipids is deposited anteriorly to the phospholipids, in accordance with the model by McCulley and Shine (5,7,8). Detailed analysis of the surface properties of the ATFLL show that the ATFLL is very stable and hardly any solubilization of the lipids takes place into the aqueous phase. This is evidenced by the very small hysteresis seen in the compression-relaxation isotherms. Furthermore, the area/molecule especially at higher surface pressures for ATFLL is too small to accommodate all lipids at the air-water interface, and thus the most likely explanation is that the nonpolar lipids (TG and CO) are deposited on top of the polar lipids. This behavior is verified by AFM (Fig. 4) and in silico (Fig. 5) studies of ATFLL, which clearly show that the nonpolar lipids are forming hemispherelike particles on the surface of the phospholipid membranes as the surface pressure is increased. At low surface pressures the nonpolar lipids are mixed within the phospholipids.

Combining the BAM and GIXD results, the main conclusion is that the ATFLL monolayer is at all pressures inhomogeneous, consisting of condensed domains which exhibit a LS structure of nontilted molecules, surrounded by a fluid phase. The bright spots observed by BAM represent the condensed islands, which (according to the GIXD observations) are composed mainly of FFA/TG, and already produced during the spreading process.

The compression-relaxation behavior of ATFLL is interesting because, during compression, part of the lipids are squeezed-out of the monomolecular film. The simulation studies show that these repulsed lipids are neutral TGs and CEs, and that, during relaxation, they are reversibly accommodated back to their original position. This excess lipid material can be considered as a lipid reservoir connected to the phospholipid monolayer, and they are associated with the reversible monolayer collapse. If only the phospholipid monolayer were considered, it is expected that it would fold into the water subphase (33–36). In this system, collapse and formation of a bilayerlike fold toward the aqueous phase decreases the free energy of the system (35,36). Yet, in ATFLL, the presence of neutral lipids on top of the phospholipids makes the difference: the free energy cost associated with folding of TGs and CEs into a globular structure rich in these lipids is minor, facilitating the formation of nonequilibrium globular structures during compression. A question remains whether similar structural folding is observed in vivo. A closer examination of the rat tear film (see Fig. 4 in (2)) shows that the lipid layer is not smooth, but instead shows distinct areas of smooth, elevated structures resembling closely the ones observed in this study, giving further evidence for the correctness and physiological significance of our model.

The C_S^{-1} values for the ATFLL and eggPC monolayers at 30 mN/m were 50 mN/m (ATFLL) and 80 mN/m (eggPC), respectively. This suggests that the ATFLL monolayer is in

a liquid-expanded phase, whereas the eggPC monolayer is in a near liquid-condensed phase during the barrier oscillation studies ($\pi = 30$ mN/m). The surface dilational modulus depends largely on the interactions between the molecules in the monolayer (38). The more condensed the monolayer, the higher the surface dilational modulus as well—which is actually observed in the difference in E between eggPC and ATFLL monolayers (Fig. 1, *C* and *D*). A higher surface dilational modulus for the more-condensed eggPC monolayers originates from stronger interaction forces between the phospholipid molecules at the interface compared to the ATFLL monolayers, for which the interaction forces between the molecules are decreased by the nonpolar molecules. However, the surface dilational modulus is not determined only by the interactions in the monolayer, but also by the structure of the monolayer (38). The lower E values for the ATFLL monolayers in relation to the eggPC monolayers may also be associated with the displacement of nonpolar molecules by the phospholipids from the interfaces, which were also shown by AFM and in silico studies of ATFLL.

The frequency dependence of the elastic and viscous components of the surface dilational modulus can be associated with the effect of the rate of deformation on the structure and stability of the eggPC and ATFLL monolayers (39). The elastic and viscous components for the eggPC monolayers as a function of frequency (Fig. 1 *C*) suggests that the merely elastic behavior of the eggPC monolayers below 25 mHz is associated with desorption and readsorption of monolayer molecules toward and from the subphase. Whereas, above 25 mHz, the visco-elastic behavior of the eggPC monolayers is more complex and is associated with a liquid-condensed to liquid-crystalline phase transition and possibly also with the formation and destruction of a three-dimensional collapsed structure during the oscillations. On the other hand, in the case of the ATFLL monolayers, the low and practically similar values for the elastic and viscous components below 50 mHz (Fig. 1 *D*) strongly suggests that the visco-elastic behavior of the monolayer originates from desorption of molecules from the interface by possibly forming small islands. This would also explain the minimum in the loss of tangent values for the ATFLL monolayers (Fig. 2), because relaxation processes such as desorption or nucleation require a time of the same magnitude as the scale of the oscillation, i.e., below 50 mHz (39). At higher frequencies ($50 < f < 200$ mHz), the visco-elastic behavior of the ATFLL monolayer could be associated with the formation/destruction of liquid-condensed domains during the oscillations.

The lipid layer of the tear fluid can be considered as viscoelastic fluid as the lipid layer of the lung surfactant. Thereby, its behavior is affected by rapid compression. This suggests that if the compression rate during a blink is high enough, the tear fluid lipid layer can experience supercompression. The compression rate of the lipid layer during a blink can be estimated rather easily if the lipid layer is approximated as a monolayer. If the change in molecular area is estimated to be, for example, as small as 10 Å^2/molecule between the fully expanded and the fully compressed states, the compression rate would be ~7000 Å^2 molecule^{-1} min^{-1}. According to this compression rate estimation, the tear film lipid layer experiences a compression rate that is considered as a supercompression ($\geq$300 Å^2 molecule^{-1} min^{-1}). If the lipid layer experiences supercompression during the downsweep of the lid, it possibly reaches a metastable state similar to that of lung surfactant. This state, holding the molecular disorder of fluid and the inability of a solid to flow, possibly prevents the extensive collapse of the lipid layer during the downsweep, and thus, provides faster spreading of the lipid layer after the upsweep.

Interestingly, the lung surfactant shares several typical characteristics with the tear fluid. In both systems, the epithelial cells are covered with a thin lining of fluid and anterior to these, both fluids have a lipid layer. And in both systems, the aqueous phase is a complex mixture of lipids and proteins, in which an active lipid-protein interacting network is formed. In the lungs the absence of the surfactant causes collapse of the alveoli because of the very high surface tension and small radius of the alveolus, and in the tear fluid the absence of the lipid layer causes increased evaporation of the water-component leading to desiccation of the corneal epithelium.

There are, however, very important distinctive features in these systems. First of all, the lung surfactant is thought to be a monolayer of phospholipids, mainly saturated dipalmitoyl-phosphatidylcholine. More interestingly, during breathing, the compression and relaxation cause a monolayer-to-bilayer transition, which is folding toward the aqueous phase (35,36). In the tear fluid, the lipids are organized into a sandwichlike structure where the phospholipids are found adjacent to the aqueous phase, and the nonpolar lipids (TGs and CEs) are deposited on top of the phospholipids. Furthermore, during compression and relaxation (mimicking blinking), the lipid-interface folds reversibly toward the air and forms spherical structures where nonpolar lipids are packed into globular structures.

SUPPORTING MATERIAL

One figure and additional materials and methods are available at http://www.biophysj.org/biophysj/supplemental/S0006-3495(10)00930-6.

This work was supported by funding from the Sigrid Juselius Foundation (to J.M.H.), the Finnish Eye Foundation (to J.M.H.), the Academy of Finland (to I.V. and J.M.H.), and Helsinki University Research Funds (to S.K.W.).

REFERENCES

1. Moss, S. E., R. Klein, and B. E. Klein. 2008. Long-term incidence of dry eye in an older population. *Optom. Vis. Sci.* 85:668–674.

2. Chen, H. B., S. Yamabayashi, …, S. Tsukahara. 1997. Structure and composition of rat precorneal tear film. A study by an in vivo cryofixation. *Invest. Ophthalmol. Vis. Sci.* 38:381–387.
3. Gipson, I. K. 2007. The ocular surface: the challenge to enable and protect vision: the Friedenwald lecture. *Invest. Ophthalmol. Vis. Sci.* 48:4390–4398.
4. Nicolaides, N., J. K. Kaitaranta, …, R. E. Smith. 1981. Meibomian gland studies: comparison of steer and human lipids. *Invest. Ophthalmol. Vis. Sci.* 20:522–536.
5. McCulley, J. P., and W. E. Shine. 2004. The lipid layer of tears: dependent on meibomian gland function. *Exp. Eye Res.* 78:361–365.
6. Greiner, J. V., T. Glonek, …, C. D. Leahy. 1996. Meibomian gland phospholipids. *Curr. Eye Res.* 15:371–375.
7. McCulley, J. P., and W. E. Shine. 1997. A compositional based model for the tear film lipid layer. *Trans. Am. Ophthalmol. Soc.* 95:79–88, discussion 88–93.
8. McCulley, J. P., and W. E. Shine. 1998. Meibomian secretions in chronic blepharitis. *Adv. Exp. Med. Biol.* 438:319–326.
9. Kaganer, V. M., H. Möhwald, and P. Dutta. 1999. Structure and phase transitions in Langmuir monolayers. *Rev. Mod. Phys.* 71:779–819.
10. Smaby, J. M., and H. L. Brockman. 1987. Regulation of cholesteryl oleate and triolein miscibility in monolayers and bilayers. *J. Biol. Chem.* 262:8206–8212.
11. Brockman, H. L., C. M. Jones, …, D. E. Jarvis. 1980. Application of a microcomputer-controlled film balance system to collection and analysis of data from mixed monolayers. *J. Colloid Interface Sci.* 78:1980502–1980512.
12. Smaby, J. M., V. S. Kulkarni, …, R. E. Brown. 1996. The interfacial elastic packing interactions of galactosylceramides, sphingomyelins, and phosphatidylcholines. *Biophys. J.* 70:868–877.
13. Kaganer, V. M., I. R. Peterson, …, P. Dutta. 1995. Tilted phases of fatty acid monolayers. *J. Chem. Phys.* 102:9412–9422.
14. Jacquemain, D., F. Leveiller, …, J. Als-Nielsen. 1991. Crystal structure of self-aggregates of insoluble aliphatic amphiphilic molecules at the air-water interface. An x-ray synchrotron study. *J. Am. Chem. Soc.* 113:7684–7691.
15. Als-Nielsen, J., D. Jaquemain, …, L. Leiserowitz. 1994. Principles and applications of grazing incidence x-ray and neutron scattering from ordered molecular monolayers at the air-water interface. *Phys. Rep.* 246:251–313.
16. Kjaer, K. 1994. Some simple ideas on x-ray reflection and grazing-incidence diffraction from thin surfactant films. *Physica B.* 198:100–109.
17. Brezesinski, G., A. Dietrich, …, H. Möhwald. 1995. Influence of ether linkages on the structure of double-chain phospholipid monolayers. *Chem. Phys. Lipids.* 76:145–157.
18. Henon, S., and J. Meunier. 1991. Microscope at the Brewster angle—direct observation of 1st-order phase-transitions in monolayers. *Rev. Sci. Instrum.* 62:936–939.
19. Hönig, D., and D. Möbius. 1991. Direct visualization of monolayers at the air-water interface by Brewster-angle microscopy. *J. Phys. Chem.* 95:4590–4592.
20. Hönig, D., G. A. Overbeck, and D. Möbius. 1992. Morphology of pentadecanoic acid monolayers at the air/water interface studied by BAM. *Adv. Mater.* 4:419–424.
21. Marrink, S. J., H. J. Risselada, …, A. H. de Vries. 2007. The MARTINI force field: coarse grained model for biomolecular simulations. *J. Phys. Chem. B.* 111:7812–7824.
22. Marrink, S. J., A. H. de Vries, and A. E. Mark. 2004. Coarse grained model for semi-quantitative lipid simulations. *J. Phys. Chem. B.* 108:750–760.
23. Koivuniemi, A., M. Heikelä, …, M. T. Hyvönen. 2009. Atomistic simulations of phosphatidylcholines and cholesteryl esters in high-density lipoprotein-sized lipid droplet and trilayer: clues to cholesteryl ester transport and storage. *Biophys. J.* 96:4099–4108.
24. Catte, A., J. C. Patterson, …, J. P. Segrest. 2008. Structure of spheroidal HDL particles revealed by combined atomistic and coarse-grained simulations. *Biophys. J.* 94:2306–2319.
25. Berendsen, H. J. C., D. van der Spoel, R., and R. van Drunen. 1995. GROMACS: a message-passing parallel molecular dynamics implementation. *Comput. Phys. Commun.* 91:43–56.
26. Van Der Spoel, D., E. Lindahl, …, H. J. Berendsen. 2005. GROMACS: fast, flexible, and free. *J. Comput. Chem.* 26:1701–1718.
27. Hess, B., C. Kutzner, …, E. Lindahl. 2008. GROMACS 4: algorithms for highly efficient, load-balanced, and scalable molecular simulation. *J. Chem. Theory Comput.* 4:435–447.
28. Berendsen, H. J. C., J. P. M. Postma, …, J. R. Haak. 1984. Molecular dynamics with coupling to an external bath. *J. Chem. Phys.* 81: 3684–3690.
29. Baoukina, S., L. Monticelli, …, D. P. Tieleman. 2007. Pressure-area isotherm of a lipid monolayer from molecular dynamics simulations. *Langmuir.* 23:12617–12623.
30. Holopainen, J. M., H. L. Brockman, …, P. K. Kinnunen. 2001. Interfacial interactions of ceramide with dimyristoylphosphatidylcholine: impact of the N-acyl chain. *Biophys. J.* 80:765–775.
31. Ihalainen, P., and J. Peltonen. 2004. Immobilization of streptavidin onto biotin-functionalized Langmuir-Schaefer binary monolayers chemisorbed on gold. *Sens. Act. B.* 102:207–218.
32. Jauhiainen, M., N. L. Setälä, …, J. M. Holopainen. 2005. Phospholipid transfer protein is present in human tear fluid. *Biochemistry.* 44: 8111–8116.
33. Lipp, M. M., K. Y. C. Lee, …, A. J. Waring. 1998. Coexistence of buckled and flat monolayers. *Phys. Rev. Lett.* 81:1650–1653.
34. Gopal, A., and K. Y. C. Lee. 2001. Morphology and collapse transitions in binary phospholipid monolayers. *J. Phys. Chem. B.* 105:10348–10354.
35. Baoukina, S., L. Monticelli, …, D. P. Tieleman. 2007. The molecular mechanism of monolayer-bilayer transformations of lung surfactant from molecular dynamics simulations. *Biophys. J.* 93:3775–3782.
36. Baoukina, S., L. Monticelli, …, D. P. Tieleman. 2008. The molecular mechanism of lipid monolayer collapse. *Proc. Natl. Acad. Sci. USA.* 105:10803–10808.
37. Reference deleted in proof.
38. Patino, J. M. R., M. R. R. Niño, and C. C. Sânchez. 2002. Static and dynamic properties of whey protein isolate and monoglyceride mixed films at the air-water interface. *Ind. Eng. Chem. Res.* 41:2652–2661.
39. Patino, J. M. R., C. C. Sânchez, …, M. C. Fernandêz. 2001. Structural dilational characteristics relationships of monoglyceride monolayers at the air-water interface. *Langmuir.* 17:4003–4013.